International Journal of Biological Macromolecules 127 (2019) 297–305

Contents lists available at ScienceDirect

International Journal of Biological Macromolecules

journal homepage: http://www.elsevier.com/locate/ijbiomac

Allura red rapidly induces amyloid-like fibril formation in hen egg white lysozyme at physiological pH

Nasser Abdulatif Al-Shabib [a,*], Javed Masood Khan [a,*], Ajamaluddin Malik [b], Priyankar Sen [c], Sriroopreddy Ramireddy [d], Sudandiradoss Chinnappan [d], Salman Freeh Alamery [e], Fohad Mabood Husain [a], Aqeel Ahmad [f], Hani Choudhry [g], Mohmmad Imran Khan [g], Sayed Ali Shahzad [a]

[a] Department of Food Science and Nutrition, Faculty of Food and Agricultural Sciences, King Saud University, Riyadh, Saudi Arabia
[b] Protein Research Chair, Department of Biochemistry, College of Science, King Saud University, Riyadh, Saudi Arabia
[c] Centre for Bioseparation Technology, Vellore Institute of Technology (VIT) University, Vellore, India
[d] Department of Biotechnology, School of Biosciences and Technology, Vellore Institute of Technology, Vellore, India
[e] Center of Excellence in Biotechnology Research, Department of Biochemistry, College of Science, King Saud University, Saudi Arabia
[f] Department of Medical Biochemistry, College of Medicine, Shaqra University, Shaqra, Saudi Arabia
[g] Department of Biochemistry, Faculty of Science, King Abdulaziz University, Jeddah, Saudi Arabia

ARTICLE INFO

Article history:
Received 17 October 2018
Received in revised form 10 January 2019
Accepted 11 January 2019
Available online 14 January 2019

Keywords:
Lysozyme
Food additive dye
Allura red
Amyloid fibril
Protein aggregation and pH

ABSTRACT

Allura red (AR) is an artificial azo dye mostly used in food industries and has potential health risks. We examined the role of AR in amyloidogenesis using hen egg white lysozyme (HEWL) at pH 7.0. The amyloidogenic induction properties of AR in HEWL were identified by circular dichroism (CD), turbidity, intrinsic fluorescence, light scattering, transmission electron microscopy (TEM), and molecular dynamic simulation studies. Turbidity and light scattering measurements showed that HEWL becomes aggregated in the presence of 0.03–15.0 mM of AR at pH 7.0 but not at very low AR concentrations (0.01–0.28 mM). However, AR-induced aggregation is a kinetically rapid process, with no observable lag phase and saturation within 6 s. The kinetics results suggested that the HEWL aggregation induced by AR is very rapid. The CD results demonstrated that the total β-sheet content of HEWL was increased in the AR treated samples. The TEM results are established that AR-induced aggregates had amyloid-like structures. Molecular dynamics simulations analysis showed that the bound AR-HEWL structures were highly favored compared to unbound structures. The mechanism of AR-induced amyloid fibril formation may involve electrostatic, hydrogen bonding, and hydrophobic interactions.

1. Introduction

Proteins have a natural tendency to fold and form their native structures to exert their biological functions. Improper folding can lead to misfolding or aggregation [1,2]. Protein aggregates are categorized as fibrillar aggregates (amyloid fibril) and amorphous aggregates (aggregates without specific structures) [3,4]. Most neurodegenerative disorders such as Alzheimer's, Parkinson's, and Huntington's diseases and type II diabetes are amyloid fibril-based diseases [5,6]. Most of the proteins involved in neurodegenerative diseases are not having any sequence identity but all the proteins can forms amyloid-like aggregates [7]. Specific amino acids sequence are known to promote protein aggregation and also called as "aggregation-prone sequences". Aggregation-prone sequences mostly contain hydrophobic and uncharged amino acids [8]. Generally, amyloid fibril formation is nucleation-dependent but nucleation-independent fibril formation has also been observed [9,10]. Several adverse conditions i.e., high temperature, different pHs, surfactants, and other small molecules or ligands are known to promote amyloid fibril formation in proteins [11,12]. Among the small molecules, several dyes, particularly food dyes, were recently reported to stimulate amyloid and amorphous aggregation of proteins [13,14].

AR is a monoazo dye as approved by the Food and Drug Administration and is highly soluble in water [15]. AR gives foods an attractive red color and is utilized in the pharmaceutical and cosmetic industries. Excess consumption of AR causes allergies, toxicity, and hyperactivity in children [16]. The European food safety authority has recommended a maximum acceptable daily intake of AR of 7.0 mg/kg body weight per day [17]. Comet assays in mice showed that AR causes DNA damage [18]. AR is banned in many European countries including Belgium, Norway, Germany, Denmark, Austria, Switzerland, and Sweden [19]. Some studies showed that aromatic amine and amide functional groups

Abbreviations: Allura red, AR; Hen egg white lysozyme, HEWL; Transmission electron microscopy, TEM.

* Corresponding authors.
E-mail addresses: nalshabib@ksu.edu.sa (N.A. Al-Shabib), javedjmk@gmail.com (J.M. Khan).

https://doi.org/10.1016/j.ijbiomac.2019.01.049
0141-8130/

in chemicals and their degradation products cause serious health hazards in consumers [20]. After gastrointestinal absorption, AR enters the bloodstream and binds to proteins during its transport and metabolism. Thus, it is essential to examined the binding of AR with its transporters and other proteins.

In present study, we investigated the response of the hen egg white lysozyme (HEWL) conformation in the presence of AR at physiological pH. We have investigated the possible interaction mechanisms between AR and HEWL protein. HEWL is relatively small (14.3 kDa) with 129 amino acids and four intramolecular disulfide bridges. HEWL belongs to the $\alpha + \beta$ class of proteins and shares nearly 60% homology with human lysozyme. Human lysozyme mutants form amyloid-like aggregates and are deposited in the liver and kidney to cause hereditary non-neuropathic systemic amyloidosis [21]. HEWL also forms amyloid-like aggregates at high temperatures [22–26]. A small peptide in HEWL of nearly 49 amino acids is hydrolyzed by heating at low pH and has been recognized as the amyloidogenic core of the protein [27]. HEWL not only shares 60% homology with human lysozyme, but also exhibits folding/unfolding and amyloid fibrillation similar to that of human lysozyme [9]. Therefore, HEWL was used as a model protein to determine the role of AR in inducing amyloid fibrillation.

We have also attempted to address the HEWL–AR interaction and tried to examine the mechanism of HEWL aggregation. This will be the first reports about HEWL and AR interaction and amyloid fibril formation. To prove the possible cause of AR induced HEWL aggregation, we have used several spectroscopic (turbidity, light scattering, intrinsic fluorescence and far-UV CD), microscopic (TEM) as well as computational techniques to explore the AR induced amyloid Fibril formation. We found that low and high concentrations of AR induce amyloid-like aggregation of HEWL at physiological pH. We used several biophysical and computational techniques to characterize HEWL fibrillation in response to AR at physiological pH and identified the amino acids involved in AR-induced fibrillation. From this study, we will propose the molecular mechanisms of HEWL aggregation induced by AR for the purpose to design the potent inhibitors against amyloid aggregates.

2. Results

2.1. Turbidity measurements

The aggregation behavior of HEWL in the presence of AR at pH 7.0 was investigated by observing the change in turbidity at 650 nm. The change in turbidity at 650 nm with respect to AR concentrations (mM) at pH 7.0 was plotted as shown in Fig. 1A. The difference in turbidity of HEWL alone and that incubated with 0.005, 0.01, 0.015, and 0.02 mM of AR was negligible shown in Fig. 1C. However, turbidity increased to 0.7 in samples containing 0.03–0.1 mM of AR shown in Fig. 1A. The turbidity of samples containing 0.1–15.0 mM of AR was approximately 0.7. The turbidity of 0–15 mM AR at 650 nm is shown as baseline. The turbidity results indicate that the HEWL formed aggregates in the presence 0.3–15.0 mM of AR at pH 7.0, with insignificant signals at lower concentrations (0.005–0.02 mM) of AR.

2.2. Light scattering measurements

Light scattering measured at 650 nm after excitation at 650 nm is a key condition for examining protein aggregation in solutions. The role of AR in the aggregation of HEWL was investigated at pH 7.0 as shown in Fig. 1B. The light scattering of HEWL at 650 nm in the absence and presence of 0.005, 0.01, 0.015, and 0.02 mM of AR was insignificant shown in Fig. 1D. However, an exponential increase was observed with 0.03–0.1 mM of AR shown in Fig. 1B. In the concentration range of 0.1–15.0 mM of AR, no further change was observed, except for a small dip in scattering. No scattering was observed at different concentrations of AR in the absence of HEWL. The light scattering results reveal that AR induces aggregation in HEWL at concentrations >0.03 mM.

2.3. AR-induced HEWL aggregation kinetics

We have examined the kinetics of AR-induced aggregation in HEWL at physiological pH. Fig. 2A shows the kinetics traces of AR-induced aggregation at different AR concentrations. The kinetics were measured as light scattering at 650 nm. In the absence of AR, HEWL showed no scattering, confirming that HEWL alone did not form aggregates. In the presence of three different (0.1, 0.2, and 0.5 mM) AR concentrations, light scattering continuously increased and reached a plateau within 6 s. The light scattering pattern showed that the aggregation process does not involve a lag phase. These results suggest that the AR-induced aggregation occurred through nucleation-independent pathways. Interestingly, in AR-induced aggregation, the kinetics pattern did not greatly change as the AR concentration was changed; however, as the concentration of AR increased, light scattering increased. The kinetics results demonstrate that AR-induced aggregates increase in size in response to higher AR concentrations. Further, the AR concentration dependent change in the rate of aggregation seems not significant (Data not shown).

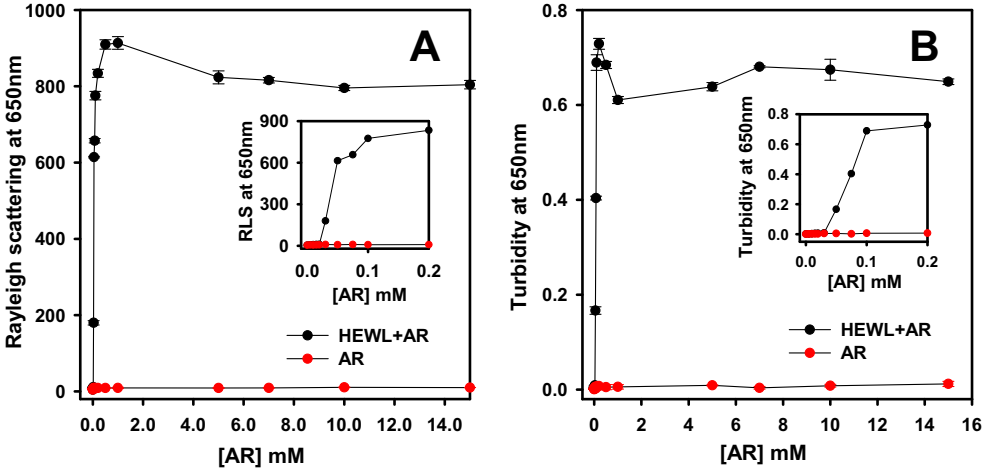

Fig. 1. Turbidity (Panel A) and light scattering (Panel B) measurements at 650 nm for samples containing HEWL+ different concentrations of AR (-■-) and different concentrations of AR alone (-●-) at pH 7.0. HEWL concentration used was 14 μM in both measurements. Lower concentrations of AR data are plotted separately as Fig. 1C (turbidity) and D (light scattering).

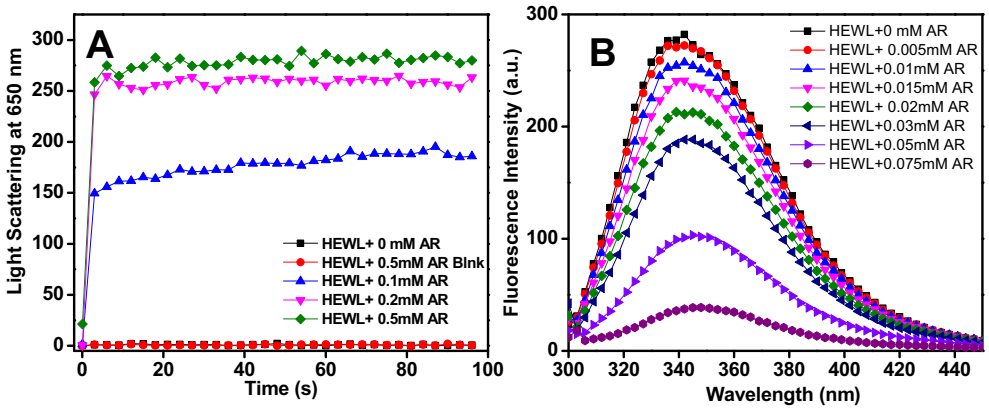

Fig. 2. A. AR-induced HEWL aggregation kinetics was measured by light scattering. Panel A showed the change in light scattering at 650 nm of a samples under different conditions i.e., HEWL alone (-■-), 0.5 mM AR only (-●-), HEWL+0.1 mM AR (-▲-), HEWL+0.2 mM AR (-▼-) and HEWL + 0.5 mM AR (-♦-) at pH 7.0. B. Intrinsic fluorescence spectra of HEWL at pH 7.0 (-■-) and with different concentrations 0.005 (-●-), 0.01 (-▲-), 0.015 (-▼-), 0.02 (-♦-), 0.03 (-◄-), 0.05 (-►-), and 0.075 (-●-) mM of AR at pH 7.0. The HEWL concentration was 14.0 μM in all measurement.

2.4. AR-induced HEWL tertiary structural changes as measured by intrinsic fluorescence

The intrinsic fluorescence of HEWL is mostly contributed by tryptophan alone. When small ligands or molecules interacted with HEWL, changes in the intrinsic fluorescence intensity and wavelength maximum were recorded around tryptophan residues [28]. The fluorescence spectra of HEWL in the absence and presence of different concentrations of AR were examined at 300–450 nm upon excitation at 295 nm, with an emission maximum at approximately 340 nm (Fig. 2B). The fluorescence intensity of HEWL decreased significantly as the AR concentration was increased from 0 to 0.075 mM. The fluorescence emission maximum was constant up to 0.03 mM AR. However, in the presence of 0.05 and 0.075 mM AR, the wavelength maximum of HEWL showed a slight red shift. The quenching in fluorescence intensity and shift in wavelength maximum indicate that HEWL aggregates in the presence high AR concentrations.

2.5. Secondary structural conformation change was monitored by CD spectroscopy

HEWL has five helical regions; three are standard alpha helices, while one (residues 109–115) is closer to the pi helix in character and two (80–84 and 120–124) are intermediate in structure between the 3–10 helix and alpha helix. There are also five beta sheet regions and large amounts of random coil and beta turns. Although this representation shows a secondary structure, its openness makes it difficult to identify the cleft. It has been reported that protein aggregation leads to conformational changes [29]; thus, changes in the secondary structure conformation were evaluated by CD spectroscopy [30,31]. The native HEWL spectrum exhibited the characteristic double minima at 208 and 222 nm, as shown in Fig. 3. These minima are characteristic features of an α-helical conformation of proteins. When HEWL was treated with a very low concentration (0.05 mM) of AR, the negative ellipticity of HEWL decreased slightly. However, in the presence of higher concentrations (0.075–1.0 mM) of AR, negative ellipticities were greatly reduced, while the shape of the spectra was not changed. The far-UV CD spectra revealed two characteristic minima (208/222 nm), but with low elipticity, which may be because of HEWL aggregation. The percent secondary structure of HEWL was calculated by K2D2 (Table 1). Native HEWL contains both α (26.47) and β (19.07) secondary structures. The percent α-helicity of HEWL was reduced in the presence of AR as the β-sheet structure increased. The details of the α to β conversion in HEWL in response to AR are shown in Table 1.

2.6. Morphology HEWL aggregates were characterized by TEM

TEM was conducted to confirm the morphology of AR-induced HEWL aggregates. TEM images of samples containing HEWL alone (Fig. 4A) and 0.1 and 0.5 mM of AR at pH 7.0 are shown in Fig. 4B and C. The HEWL without AR not showing any aggregation. The results showed in Fig. 4B and C that HEWL formed rod-like fibrils in the presence of AR. The fibrils sizes were not identical in the presence of both the concentrations. The average fibril length 1640 ± 10 nm and thickness 14.54 ± 2.9 nm was found in the presence of both the concentrations of AR. These TEM results support the finding that AR induced amyloid-like aggregates in HEWL at pH 7.0. Based on these results, we conducted molecular dynamics simulation to evaluate the intra-residual interaction and their atomistic behavior in structural folding among bound-unbound complexes.

2.7. Conformational differences in stability and flexibility between HEWL bound-unbound states

The interacting mechanism of bound (HEWL-AR) and unbound (HEWL) was visualized by molecular docking. According to the binding constant principle, lower the binding energy of the ligand indicates

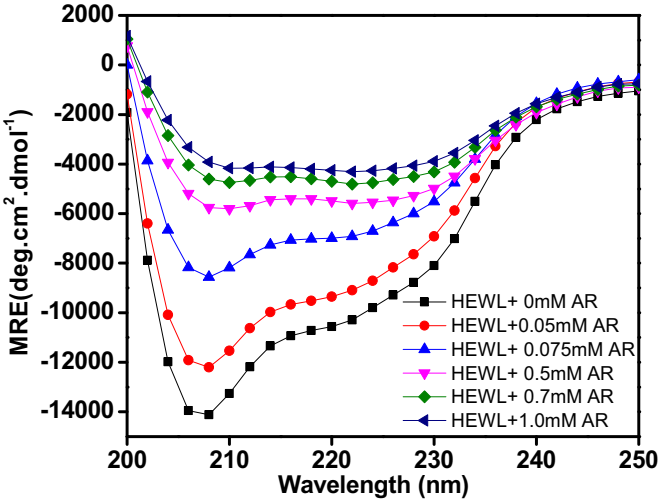

Fig. 3. Far-UV CD spectra (panel A) of HEWL (14 μM) were measured under different conditions, i.e. pH 7.0 (-■-) and in the presence of 0.05 (-●-), 0.075 (-▲-), 0.5 (-▼-), 0.7 (-♦-), and 1.0 (-◄-) mM of AR at pH 7.0.

Table 1
Percent secondary structural change in HEWL in response to AR concentrations at pH 7.0.

S. no.	Conditions	Alpha-helix	Beta-sheet
1	HEWL + 0.0 AR	26.47 ± 1.02	19.07 ± 0.62
2	HEWL + 0.05 mM AR	23.7 ± 0.82	26.2 ± 0.72
3	HEWL + 0.075 mM AR	20.46 ± 0.41	29.8 ± 0.70
4	HEWL + 0.5 mM AR	10.0 ± 0.27	40.55 ± 0.94
5	HEWL + 0.7 mM AR	3.80 ± 0.05	49.02 ± 1.09
6	HEWL + 1.0 mM AR	3.80 ± 0.01	49.02 ± 1.82

higher efficacy. The results are shown in Table 2. We also observed interacting amino acids within 4 Å, revealing how AR interacts with the protein during aggregation, as shown in Fig. 5A. Whereas, Fig. 5B states the interacting amino acid residues with the bond distance between AR-and HEWL. Additionally, the bound (HEWL-AR) unbound states (HEWL) were analyzed by Gromacs parameterization of the trajectory files. The parameter rmsd was used to obtain the structural information on conformational co-operativity for backbone leading to stability. The native unbound form (HEWL) was well-stabilized after 8 ns with an rmsd of 0.1 nm, whereas the bound complex (HEWL-AR) showed minimal distractions in convergence after 20 ns an rmsd 0.15 nm and showed stable values at 0.2 nm. Hence, the convergence gives us a clear view that native as well as the complex attaining steady transition state and maintaining equilibrium. The results revealed that both the bound and unbound structures converged well with a minimal deviation of approximately 20 ns equilibration. Fig. 6A also confirms that the complexes (bound-unbound) were stable following exposure to AR. The parameter rmsf was used to evaluate the residual fluctuations in the C-α region of the overall average structural conformation and the graph was generated as an average native and complex for the time scale. In Fig. 6B, the rmsf of the bound (HEWL-AR) complex revealed higher flexibility in the N-terminal (1–60, 79–83, and 96–100) and C-terminal regions (105–129) compared to unbound (HEWL). This flexibility may enable AR to favor complex formation compared to the unbound complex, supporting our results obtained by analyzing the bound complex. Accordingly, the conformational changes were significantly observed in unbound and bound states of HEWL, through various geometrical parameters, which substantiated the difference in conformational deviation and flexibility, thus stipulating a root cause for aggregation.

2.8. Structural compactness and hydrogen bond formation instability factors of HEWL-AR

The SASA is a critical parameter revealing the conformational compactness of a bimolecular structure and accessible to a solvent; depends on the hydrophobic core which helps preserve the native fold. Here, we compared the SASA between the bound (HEWL-AR) and unbound states (HEWL) from the trajectories as shown in Fig. 7A. The unbound form (HEWL) exhibited a surface area of ~32–36 nm^2 in a simulation of ~2–25 ns, while the bound form (HEWL-AR) showed a SASA of ~34–35 nm^2 for the first 5 ns in contrast to the unbound structure, after which the surface area was dramatically reduced to ~30–34 nm^2 and maintained throughout the simulation. The reduced SASA indicates differences in exposed amino acid residues which may avert the tertiary structure packing of the structural architecture. Hydrogen bonding interaction analysis is essential for examining structural stabilization. Fig. 7B shows that the bound complex (HEWL-AR) maintained stable due to 5–6 hydrogen bonds. The simulation results clearly indicated that the amino acids residues particularly Ala-Ile-Ser-Asp-Asn-Cys (78–93) are involved in hydrogen bonding and forming the complex more stable. This hydrogen bond formation may promote dramatic changes that influence HEWL structural integration and stabilization linked to aggregation-related folding. Fig. 7B shows that the bound complex (HEWL-AR) maintained stable due to 5–6 hydrogen bonds. The simulation results indicated that the amino acids residues in HEWL, i.e. Ala-Ile-Ser-Asp-Asn-Cys (78–93) particularly are involved in hydrogen bond and forming the complex. This hydrogen bond formation may promote dramatic changes that influence HEWL structural integration and stabilization linked to aggregation-related folding [32–34]. Moreover, our results corroborated with the experimental studies on the aggregation activity.

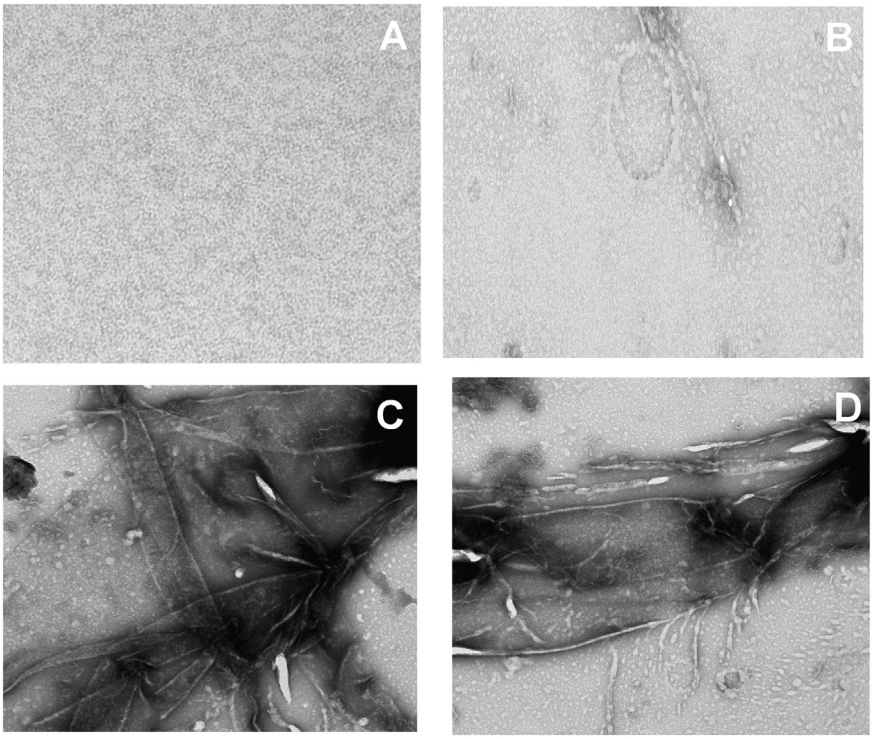

Fig. 4. Transmission electron microscopy images of HEWL aggregates. Panels A, B, C and D show HEWL (0.2 mg mL^{-1}) without and with 0.02, 0.1 and 0.5 mM AR at pH 7.0.

Table 2
Docking score and interacting residues between HEWL-AR.

Compound	Binding energy	Total internal energy	Amino acids involved in H-bonding	Neighboring amino acid residues
AR	−5.77 (kCal/mol)	−1.32 (kCal/mol)	Asp87, Ser85, Ala90, Asn 93	Cys76, Ile78, Ser85, Ile88, Thr89, Cys94, Lys96, Lys97

3. Discussion

In this study, we examined the properties of interactions between the negatively charged food dye AR and the protein HEWL at physiological pH and characterized the amyloid fibril formation of HEWL. AR is a negatively charged food dye, while HEWL is positively charged at physiological pH [11,14]. Numerous studies have shown that negatively charged ligands interact electrostatically with proteins to result in amyloid-like fibril formation [35,36]. We characterized the role of AR in HEWL aggregation resulting in amyloid fibril formation using spectroscopic and microscopic techniques.

Our turbidity and light scattering results showed that the HEWL formed aggregates in the presence of 0.03–15.0 mM of AR at pH 7.0. However, no aggregation was observed at below 0.03 mM of AR. The increase in turbidity indicated that AR induces bigger size aggregates. Similar observation is also recorded in other published reports, i.e., the turbidity of transforming growth factor-β3 was found to be directly proportional to protein concentration at pH 7.5 [37]. The turbidity and light scattering measurements confirmed that AR induced aggregation of HEWL at pH 7.0. The kinetics results showed that AR-induced aggregation was nucleus-independent because the lag phase was completely absent in the presence of AR. The kinetics pattern suggests that the monomer of HEWL is stable in the absence of AR, while in the presence of AR, the monomer HEWL immediately forms large oligomers as aggregates. Aggregate formation is very rapid, with saturation achieved within a few seconds. Similar kinetics results were observed for Tau (Tau4RD) protein when Tau was treated with heparin [38]. The Tau monomer directly converted into amyloid-like aggregates without a lag phase [38]. Intrinsic fluorescence measurements revealed the position of tryptophan residues during AR-induced aggregation [14,39]. The fluorescence intensity was quenched and the wavelength maximum of HEWL was red-shifted when AR bound to HEWL. These results indicate that HEWL had aggregated and agreed with the results of previous studies showing that the wavelength maximum was slightly red-shifted when AR interacted with human serum albumin [40]. The secondary structure of HEWL was also affected by AR-induced aggregation. It was reported that the α-helical structure of a protein is converted into a β-sheet or cross β-sheet structure upon protein aggregation [41]. HEWL alone showed two minima at 208 and 222 nm, which are characteristic features of α-helical proteins at pH 7.0 [42]. The ellipticity of HEWL becomes greatly reduced in the presence of AR at physiological pH. The minima of HEWL at 208 and 222 nm are also distorted in the presence of AR. The percent secondary structure was also calculated by online software K2D2 methods described in CD methodology. From the K2D2 calculation, it was noted that the percent β-sheet structures increased and decreased in α-helicity in the presence of AR. The increase in β-sheet structures and decrease in α-helical structures was attributed to the formation of HEWL aggregates with a definite morphology. The secondary structure measurements confirmed that the aggregates generated by AR have definite morphologies known as amyloid fibrils. The results from computational studies also stated the increase in β-sheet content which are conceded by the experimental results [52]. Additionally, amyloid-like aggregates have high β-sheet contents compared to non-amyloid aggregates [43,44]. In addition, we also elucidated the variations in the secondary structural parameters of the bound AR-HEWL protein state to differentiate the aggregation from our simulation studies [45]. Overall secondary structural changes showed that the AR-induced aggregates were amyloid-like. The morphology of AR-induced aggregates was further confirmed by TEM, which supported that the AR-induced the formation of amyloid-like aggregates. The fibril size are almost identical in both the concentrations of AR, length 1640 ± 10 nm and width is almost 14.54 ± 2.9 nm.

Fig. 8 shows a proposed mechanism of AR-induced aggregation in HEWL. HEWL has a net charge of approximately +7 at pH 7.0 as determined by PROTEIN CALCULATOR v3.4 software. The isoelectric point of HEWL was reported to be approximately 11.0 [46]; however, below pH 11.0, HEWL is positively charged because arginine, lysine, and histidine are protonated. The negatively charged sulfate group of AR interacts electrostatically with protonated amino acids of HEWL and neutralizes the HEWL charges. Because of this charge neutralization, the HEWL-solvent interaction is perturbed and new HEWL-HEWL or HEWL-AR-HEWL interactions increase, leading to HEWL aggregation. Other negatively charged sulfate groups interact via electrostatic interactions with positively charged amino acids in HEWL to induce amyloid-like fibril formation at low pH [47]. Molecular dynamics simulation showed that the bound AR, which corresponds to conformational transition, fluctuation, and compactness, promoted aggregation of HEWL. Moreover, AR can bind to HEWL and act as a competitive substrate.

4. Experimental section

4.1. Materials

HEWL, AR, and other chemicals were obtained from Sigma. Other chemicals and reagents used in this study were of analytical grade with purity >99%. All solutions (protein, dyes, and other reagents) were filtered through a 0.45-μm syringe filter (Millipore, Billerica, MA, USA). The HEWL stock was prepared in 20 mM Tris-HCl buffer pH 7.0 and

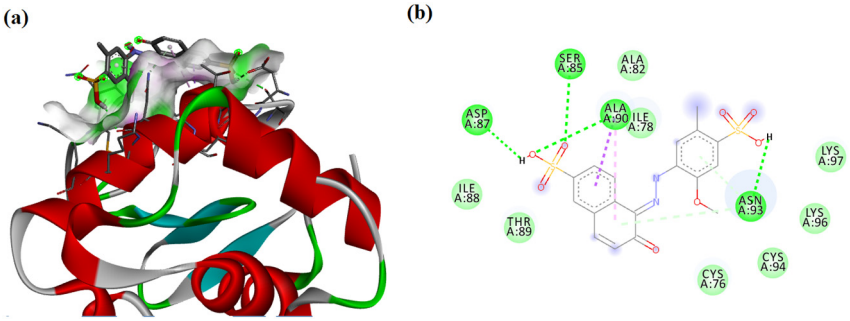

Fig. 5. (A) Docking complex (HEWL-AR). (B) 2-D plot of interacting residual contacts of HEWL and AR.

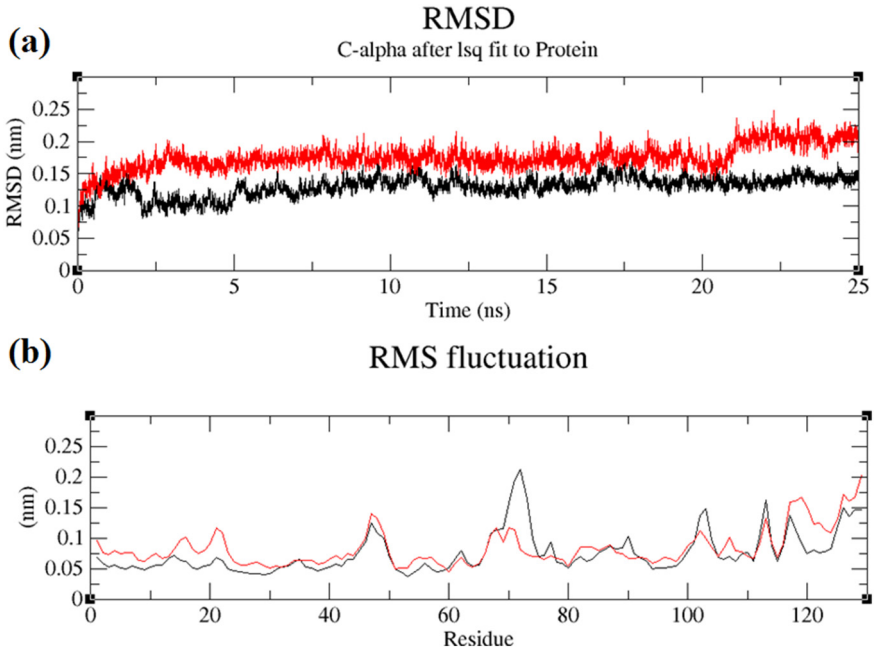

Fig. 6. (A) Root mean square deviation of backbone atoms unbound (black) and bound complex of HEWL-AR (red). (B) Cα-RMSF (root-mean-square fluctuation) of unbound (black) and bound complex of HEWL-AR (red).

the concentration was calculated using an Agilent Technologies Carry 60 UV–visible spectrophotometer (Santa Clara, CA, USA) and a molar extinction coefficient of 37,970 M^{-1} cm^{-1} at 280 nm.

4.2. Turbidity measurements

The turbidity of HEWL (0.2 mg mL^{-1}) in the presence and absence of AR in the concentration range (0–15.0 mM) at pH 7.0 was measured at 650 nm. Measurements were performed using an Agilent Technologies Carry 60 UV–visible spectrophotometer. Before taking the turbidity reading, HEWL samples with AR were incubated overnight at different pH levels.

4.3. Light scattering measurements

Light scattering measurement was carried out to characterize AR-induced aggregation in HEWL at pH 7.0. The Carry Eclipse fluorescence spectrophotometer at 25 °C was used for light scattering measurements

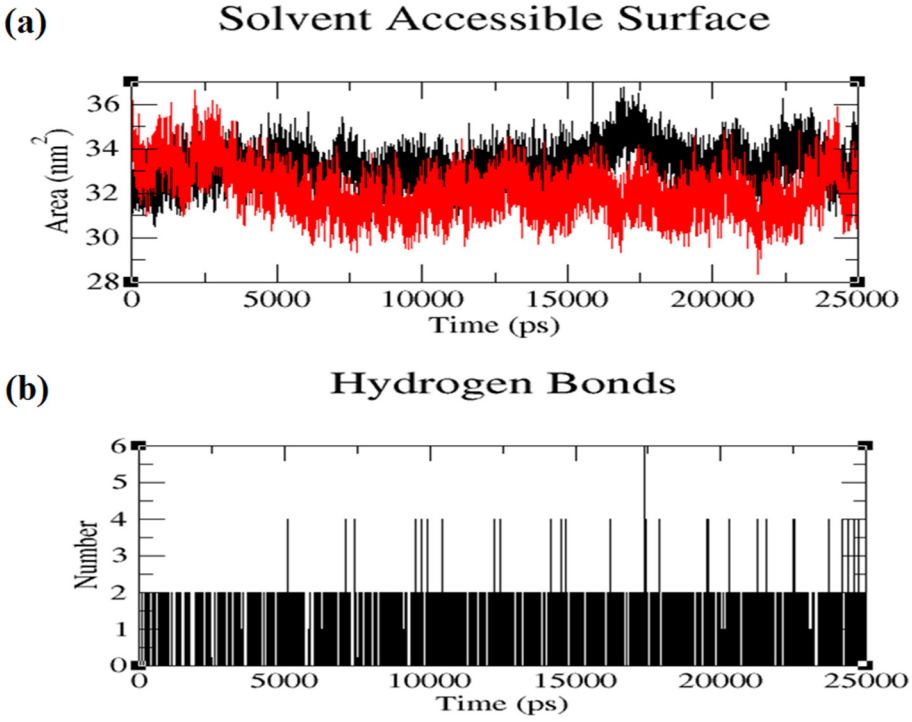

Fig. 7. (A) SASA of unbound (HEWL) and bound (HEWL-AR) structures for 25-ns trajectory. This shows the projection of exposed areas of unbound (black) and bound complex of HEWL-AR (red). (B) Hydrogen bond analysis. Hydrogen bond formation between HEWL-AR.

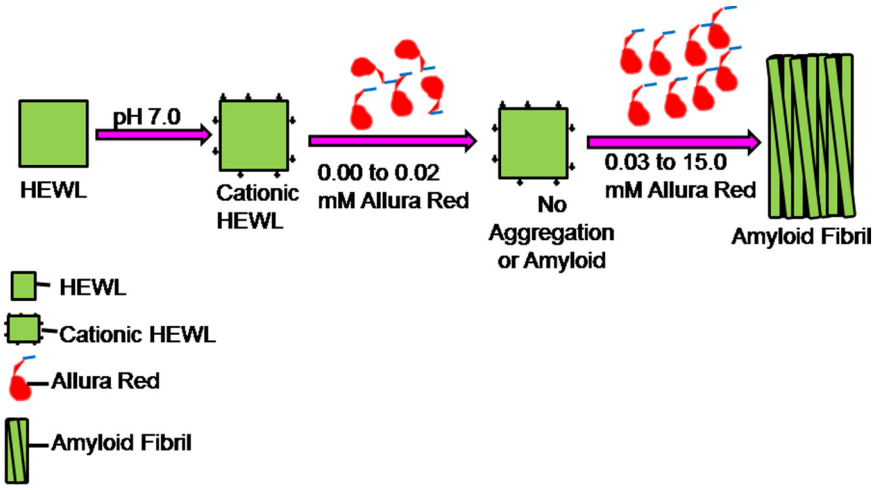

Fig. 8. Schematic illustration of AR-induced fibrillation of HEWL at pH 7.0.

in a 1.0-cm path length cuvette. HEWL (0.2 mg mL^{-1}) was incubated with different concentrations of AR (0–15 mM) at pH 7.0. The HEWL samples with and without AR were excited at 650 nm and emission was recorded at 650 nm.

4.4. AR-induced aggregation kinetics

Kinetics analysis of AR-induced HEWL aggregation was conducted on a Carry Eclipse fluorescence spectrofluorometer attached to Peltier and a stirrer at a constant speed at room temperature in a 3-mL cuvette with a 1-cm path length. HEWL samples with and without AR were excited at 650 nm and emission was recorded at the same wavelength with respect to time in seconds. The excitation and emission slit widths were fixed to 1.5 and 2.5 nm and the HEWL concentration was 0.2 mg mL^{-1}. All kinetics measurements were performed at pH 7.0.

4.5. Intrinsic fluorescence measurements

Intrinsic fluorescence measurements were carried out on Carry Eclipse fluorescence spectrofluorometer at room temperature in a 1-cm path length cuvette. HEWL (0.2 mg mL^{-1}) was incubated with AR (0.005–0.075 mM) at pH 7.0. HEWL samples with and without AR were excited at 295 nm and emission spectra were recorded over a wavelength range of 300–450 nm. The excitation and emission slit widths were fixed at 5 nm. We measured intrinsic fluorescence at lower concentrations of AR to avoid dye interference.

4.6. Far-UV CD measurements

Far-UV CD was conducted to measure the change in the secondary structure of HEWL in response to AR. The far-UV CD was measured on an Applied Photophysics Chirascan-Plus (Leatherhead, UK) spectropolarimeter attached to a Peltier. Far-UV CD spectra of all samples incubated with and without AR were scanned in the range of 200–250 nm. HEWL (0.2 mg mL^{-1}) was treated with various concentrations of AR overnight. HEWL incubated 0.2 mM AR was centrifuged at 10000 RPM for 5 min. After centrifugation, the supernatant was discarded and precipitates were dissolved in pH 7.0 buffer. The samples were centrifuged to remove excess dye. The centrifuged and non-centrifuged samples were scanned three times over 200–250 nm and the average spectra were taken. The averaged spectra were smoothed by the Savitzky–Golay method.

The far-UV CD results were expressed as mean residual ellipticity and secondary structure were calculated by K2D2 methods [48].

4.7. Transmission electron microscopy (TEM)

TEM was conducted to determine the morphology of AR-induced aggregates of HEWL. A JEOL transmission electron microscope (JEOL JEM-1011, Tokyo, Japan) operating at an accelerating voltage of 120 kV was used to capture images of the aggregates. HEWL (0.2 mg mL^{-1}) was treated with 0.1 and 0.5 mM of AR at pH 7.0 and incubated overnight. The 12.0 μL of AR-induced HEWL aggregate samples were applied to a 200-mesh copper grid. The grid was negatively stained with 2% (w/v) uranyl acetate and dried in a desiccator.

4.8. Docking analysis of HEWL-AR

The 3D structure of HEWL was obtained from RCSB-PRotein Data bank (PDB id: 2LYZ), and the ligand was obtained from PubChem compound with a unique compound CID id: 5360805. The 3D structures were preprocessed and prepared for docking process. We used a standard docking protocol to form stable HEWL-AR complexes [49]. *Autodock 4.2* software was used for docking calculations [50]. Firstly, the protein PDB structure was processed by recognizing the bond distances, addition of the polar and non-polar hydrogens and applying the force field for proper orientation of the amino acids with the structure. Later, the Kollman and gasteiger charges were assigned for calibration of structural changes and saving the final processed structure in a pdbqt format. The torsions of the ligand were processed making it ready for the utilization for the complex formation. The protein HEWL and ligand AR were identified (for 10 independent runs per ligand). A grid box was calibrated around the active site with dimensions of 60 × 60 × 60 points on the x, y, and z-axes with a grid spacing of 0.375 Å. The default values were maintained for all parameters. Later, the grid box was obtained using the Auto grid function followed by Autodock function with Lamarckian genetic algorithm for the best docking conformations. The final docking poses obtained along with the calculations of binding energies. The best conformation was obtained with the least binding energy. Thereby, a detailed analysis of hydrogen bonding was generated and visualized using Discovery Studio Visualizer (Accelrys Software, Inc., San Diego, CA, USA).

4.9. Complex molecular dynamics simulation

Gromacs 4.6.5, a molecular dynamics simulation package, was used to analyze the dynamic behavior of the HEWL-AR complex [51]. The initial steps of molecular dynamics simulation were performed using the GROMOS 53a6 forcefield [52]. The forcefield and topology parameter files of the ligand were generated using the Dundee PRODRG web

server. The water molecules were placed in complex with a simple point charge 216 model (SPC216). The system was neutralized using counterions and periodic boundary conditions were applied. The full system was energy-minimized while maintaining a constant temperature, pressure, and volume. The final molecular dynamics simulation was carried out for 25 ns. The final trajectory analysis was carried out using the inbuilt modules of Gromacs which include the root mean square deviation (rmsd) root mean square fluctuation (rmsf), solvent accessible surface area (SASA), and hydrogen bonds. These analyses provided valuable insight into the activity of AR towards HEWL.

5. Conclusions

In this study, we showed that AR-induces amyloid-like aggregate formation of HEWL at pH 7.0. HEWL formed amyloid-like fibrils very rapidly in the presence of 0.03–15.0 mM of AR. The α-helical structure of HEWL was reduced in the presence of AR with a concomitant increase in β-sheet structures. The AR-induced amyloid fibrillation of HEWL occurred through electrostatic interactions between positively charged amino acids (arginine, lysine and histidine) of HEWL and negatively charged sulfate groups of AR. The electrostatic interaction between positively charged amino acids and AR is not possible till positively charged amino acids are protonated. Computational methods were used to determine the dynamic transition state, which revealed the site of interaction between HEWL and other amino acids surrounding AR. Thus, we provide a detailed description of the formation of amyloid-like aggregates of HEWL.

Acknowledgments

The authors extend their appreciation to Deanship of Scientific Research at King Saud University for funding this work through Research Group no. RGP-1439-014.

Author contributions

Javed Masood Khan designed the experiments; Javed Masood Khan, Nasser Abdulatif Al-Shabib, Ajamaluddin Malik, Sriroopreddy Ramireddy, Sudandiradoss C, Salman Freeh Alamery, Fohad Mabood Husain, performed the experiments; Javed Masood Khan analyzed the data; Javed Masood Khan and Nasser Abdulatif Al-Shabib wrote the manuscript; and Javed Masood Khan, Ajamaluddin Malik, Priyankar Sen, Aqeel Ahmad Review & Editing.

Conflicts of interest

The authors declare no conflict of interest.

References

[1] J.M. Yon, Protein folding in the post-genomic era, J. Cell. Mol. Med. 6 (2002) 307–327.
[2] L.F. Agate, D. Guidolin, G. Leo, S. Genedani, P. Arhem, A. Forni, et al., Role of cooperativity in protein folding and protein mosaic assemblage relevance for protein conformational diseases, Curr. Protein Pept. Sci. 8 (2007) 460–470.
[3] S.S.S. Wang, T.A. Good, An overview of Alzheimer's disease, J. Ind. Eng. Chem. 36 (2005) 533–559.
[4] V.N. Uversky, A.L. Fink, Conformational constraints for amyloid fibrillation: the importance of being unfolded, Biochim. Biophys. Acta 1698 (2004) 131–153.
[5] J. Pujols, S. Peña-Diaz, M. Conde-Giménez, F. Pinheiro, S. Navarro, J. Sancho, S. Ventura, High-throughput screening methodology to identify alpha-synuclein aggregation inhibitors, Int. J. Mol. Sci. 18 (3) (2017) 478.
[6] D. Morshedi, A. Ebrahim-Habibi, A.A. Moosavi-Movahedi, M. Nemat-Gorgani, Chemical modification of lysine residues in lysozyme may dramatically influence its amyloid fibrillation, Biochim. Biophys. Acta 1804 (4) (2010) 714–722.
[7] M. Biancalana, S. Koide, Molecular mechanism of thioflavin-T binding to amyloid fibrils, Biochim. Biophys. Acta 1804 (7) (2010) 1405–1412.
[8] G. De Baets, J. Schymkowitz, F. Rousseau, Predicting aggregation-prone sequences in proteins, Essays Biochem. 56 (2014) 41–52.
[9] A.P. Chaudhary, N.H. Vispute, V.K. Shukla, B. Ahmad, A comparative study of fibrillation kinetics of two homologous proteins under identical solution condition, Biochimie 132 (2017) 75–84.
[10] J.S. Cristovao, S.S. Leal, I. Cardoso, C.M. Gomes, Small molecules present in the cerebrospinal fluid metabolome influence superoxide dismutase 1 aggregation, Int. J. Mol. Sci. 14 (9) (2013) 19128–19145.
[11] J.M. Khan, M.S. Khan, M.A. Alsenaidy, A. Ahmed, P. Sen, M. Oves, et al., Sodium louroyl sarcosinate (sarkosyl) modulate amyloid fibril formation in hen egg white lysozyme (HEWL) at alkaline pH: a molecular insight study, J. Biomol. Struct. Dyn. 36 (6) (2018) 1550–1565.
[12] S.K. Chaturvedi, N. Zaidi, P. Alam, J.M. Khan, A. Qadeer, I.A. Siddique, et al., Unraveling comparative anti-amyloidogenic behavior of pyrazinamide and D-cycloserine: a mechanistic biophysical insight, PLoS One 10 (8) (2015), e0136528.
[13] N.A. Al-Shabib, J.M. Khan, M.S. Khan, M.S. Ali, A.M. Al-Senaidy, M.A. Alsenaidy, et al., Synthetic food additive dye "Tartrazine" triggers amorphous aggregation in cationic myoglobin, Int. J. Biol. Macromol. 98 (2017) 277–286.
[14] N.A. Al-Shabib, J.M. Khan, A. Malik, A.M. Alsenaidy, M.A. Alsenaidy, F.M. Husain, et al., Negatively charged food additive dye "Allura Red" rapidly induces SDS-soluble amyloid fibril in beta-lactoglobulin protein, Int. J. Biol. Macromol. 107 (Pt B) (2018) 1706–1716.
[15] D. Wu, J. Yan, J. Wang, Q. Wang, H. Li, Characterisation of interaction between food colourant Allura red AC and human serum albumin: multispectroscopic analyses and docking simulations, Food Chem. 170 (2015) 423–429.
[16] N. Pourreza, S. Rastegarzadeh, A. Larki, Determination of Allura red in food samples after cloud point extraction using mixed micelles, Food Chem. 126 (3) (2011) 1465–1469.
[17] European Food Safety Authority, Refined exposure assessment for Allura red AC (E 129), EFSA J. 13 (2) (2015) 1–33.
[18] C. Shimada, K. Kano, Y.F. Sasaki, I. Sato, S. Tsuda, Differential colon DNA damage induced by azo food additives between rats and mice, J. Toxicol. Sci. 35 (4) (2010) 547–554.
[19] K. Rovina, S. Siddiquee, S.M. Shaarani, Extraction, analytical and advanced methods for detection of Allura red AC (E129) in food and beverages products, Front. Microbiol. 7 (2016) 798.
[20] F. Gosetti, U. Chiuminatto, E. Mazzucco, G. Calabrese, M.C. Gennaro, E. Marengo, Non-target screening of Allura red AC photodegradation products in a beverage through ultra-high performance liquid chromatography coupled with hybrid triple quadrupole/linear ion trap mass spectrometry, Food Chem. 136 (2) (2013) 617–623.
[21] D.R. Booth, M. Sunde, V. Bellotti, C.V. Robinson, W.L. Hutchinson, P.E. Fraser, P.N. Hawkins, C.M. Dobson, S.E. Radford, C.C. Blake, M.B. Pepys, Instability, unfolding and aggregation of human lysozyme variants underlying amyloid fibrillogenesis, Nature 385 (6619) (1997) 787–793.
[22] L.N. Arnaudov, R. de Vries, Thermally induced fibrillar aggregation of hen egg white lysozyme, Biophys. J. 88 (1) (2005) 515–526.
[23] S. Nusrat, N. Zaidi, M. Zaman, S. Islam, M.R. Ajmal, M.K. Siddiqi, M.K. Santra, R.H. Khan, Repositioning nordihydroguaiaretic acid as a potent inhibitor of systemic amyloidosis and associated cellular toxicity, Arch. Biochem. Biophys. 612 (2016) 78–90.
[24] S. Nusrat, A. Masroor, M. Zaman, M.K. Siddiqi, M.R. Ajmal, N. Zaidi, A.S. Abdelhameed, R.H. Khan, Interaction of catecholamine precursor l-Dopa with lysozyme: a biophysical insight, Int. J. Biol. Macromol. 109 (2018) 1132–1139.
[25] P. Alam, S.K. Chaturvedi, M.K. Siddiqi, R.K. Rajpoot, M.R. Ajmal, M. Zaman, R.H. Khan, Vitamin k3 inhibits protein aggregation: implication in the treatment of amyloid diseases, Sci. Rep. 6 (2016), 26759.
[26] M.R. Ajmal, S.K. Chaturvedi, N. Zaidi, P. Alam, M. Zaman, M.K. Siddiqi, S. Nusrat, M.S. Jamal, M.H. Mahmoud, G. Badr, R.H. Khan, Biophysical insights into the interaction of hen egg white lysozyme with therapeutic dye clofazimine: modulation of activity and SDS induced aggregation of model protein, J. Biomol. Struct. Dyn. 35 (10) (2017) 2197–2210.
[27] E. Frare, M.F. Mossuto, P. Polverino de Laureto, M. Dumoulin, C.M. Dobson, A. Fontana, Identification of the core structure of lysozyme amyloid fibrils by proteolysis, J. Mol. Biol. 361 (2006) 551–561.
[28] D. Shasha, W. Qing, Y. Xiaohai, W. Kemin, L. Lin, L. Qing, et al., Acceleration of hen egg white lysozyme amyloid fibrillation by single- or few-layer molybdenum disulfide nanosheets, J. Nanosci. Nanotechnol. 17 (2017) 2892–2898.
[29] L. Nault, C. Vendrely, Y. Brechet, F. Bruckert, M. Weidenhaupt, Peptides that form β-sheets on hydrophobic surfaces accelerate surface-induced insulin amyloidal aggregation, FEBS Lett. 587 (2013) 1281–1286.
[30] M.K. Siddiqi, P. Alam, S. Malik, N. Majid, S.K. Chaturvedi, S. Rajan, M.R. Ajmal, M.V. Khan, V.N. Uversky, R.H. Khan, Stabilizing protein to prevent conformational changes required for amyloid fibril formation, J. Cell. Biochem. (2018) https://doi.org/10.1002/jcb.27576.
[31] S.K. Chaturvedi, J.M. Khan, M.K. Siddiqi, P. Alam, R.H. Khan, Comparative insight into surfactants mediated amyloidogenesis of lysozyme, Int. J. Biol. Macromol. 83 (2016) 315–325.
[32] E. Srinivasan, R. Rajasekaran, Exploring the cause of aggregation and reduced Zn binding affinity by G85R mutation in SOD1 rendering amyotrophic lateral sclerosis, Proteins: Struct., Funct., Bioinf. 85 (2017) 1276–1286.
[33] E. Srinivasan, R. Rajasekaran, Probing the inhibitory activity of epigallocatechin-gallate on toxic aggregates of mutant (L84F) SOD1 protein through geometry based sampling and steered molecular dynamics, J. Mol. Graph. Model. 74 (2017) 288–295.
[34] E. Srinivasan, R. Rajasekaran, Comparative binding of kaempferol and kaempferide on inhibiting the aggregate formation of mutant (G85R) SOD1 protein in familial amyotrophic lateral sclerosis: a quantum chemical and molecular mechanics study, Biofactors 44 (2018) 431–442.

[35] T.A. Kayal, S. Nappini, E. Russo, D. Berti, M. Bucciantini, M. Stefani, et al., Lysozyme interaction with negatively charged lipid bilayers: protein aggregation and membrane fusion, Soft Matter 8 (2012) 4524–4534.
[36] K.A. Burke, E.A. Yates, J. Legleiter, Biophysical insights into low surfaces, including lipid membranes, modulate protein aggregation related to neurodegeneration, Front. Neurol. 4 (2013) 17.
[37] J. Pellaud, U. Schote, T. Arvinte, J. Seelig, Conformation and self-association of human recombinant transforming growth factor-beta3 in aqueous solutions, J. Biol. Chem. 274 (12) (1999) 7699–7704.
[38] G. Ramachandran, J.B. Udgaonkar, Understanding the kinetic roles of the inducer heparin and of rod-like protofibrils during amyloidfibril formation by tau protein, J. Biol. Chem. 286 (45) (2011) 38948–38959.
[39] S. Esmaeili, M.R. Ashrafi-Kooshk, K.J. Khaledian, H. Adibi, S. Rouhani, R. Khodarahmi, Degradation products of the artificial azo dye, Allura red, inhibit esterase activity of carbonic anhydrase II: a basic in vitro study on the food safety of the colorant in terms of enzyme inhibition, Food Chem. 213 (2016) 494–504.
[40] L. Wang, G. Zhang, Y. Wang, Binding properties of food colorant Allura red with human serum albumin in vitro, Mol. Biol. Rep. 41 (5) (2014) 3381–3391.
[41] A. Basu, G.S. Kumar, Interaction and inhibitory influence of the azo dye carmoisine on lysozyme amyloid fibrillogenesis, Mol. BioSyst. 13 (2017) 1552–1564.
[42] T.M. Ryan, G.J. Howlett, M.F. Bailey, Fluorescence detection of a lipid-induced tetrameric intermediate in amyloid fibril formation by apolipoprotein C-II, J. Biol. Chem. 283 (50) (2008) 35118–35128.
[43] R. Krishnan, S.L. Lindquist, Structural insights into a yeast prion illuminate nucleation and strain diversity, Nature 435 (2005) 765–772.
[44] M. Adachi, M. So, K. Sakurai, J. Kardos, Y. Goto, Supersaturation-limited and unlimited phase transitions compete to produce the pathway complexity in amyloid fibrillation, J. Biol. Chem. 290 (29) (2015) 18134–18145.
[45] E. Srinivasan, R. Rajasekaran, Quantum chemical and molecular mechanics studies on the assessment of interactions between resveratrol and mutant SOD1 (G93A) protein, J. Comput. Aided Mol. Des. (2018) 1–15.
[46] O. Zschörnig, G. Paasche, C. Thieme, N. Korb, K. Arnold, Modulation of lysozyme charge influences interaction with phospholipid vesicles, Colloids Surf. B: Biointerfaces 42 (1) (2005) 69–78.
[47] J.M. Khan, S.K. Chaturvedi, S.K. Rahman, M. Ishtikhar, A. Qadeer, E. Ahmad, et al., Protonation favors aggregation of lysozyme with SDS, Soft Matter 10 (2014) 2591–2599.
[48] J.M. Khan, M.R. Khan, p. Sen, A. Malik, M. Irfan, R.H. Khan, An intermittent amyloid phase found in gemini (G5 and G6) surfactant induced β-sheet to α-helix transition in concanavalin A protein, J. Mol. Liq. 269 (2018) 796–804.
[49] R. Sriroopreddy, P. Raghuraman, R.B. Reena, Modeling and docking study of GABA-AT protein in *Mycobacterium tuberculosis* - a computational approach, Res. J. Pharm. Technol. 11 (2018) 1283–1288.
[50] G.M. Morris, R. Huey, W. Lindstrom, M.F. Sanner, R.K. Belew, et al., {AutoDock}4 and {AutoDockTools}4: automated docking with selective receptor flexibility, J. Comput. Chem. 30 (16) (2009) 2785–2791.
[51] S. Pronk, S. Páll, R. Schulz, P. Larsson, P. Bjelkmar, et al., GROMACS 4.5: a high-throughput and highly parallel open source molecular simulation toolkit, Bioinformatics 29 (2013) 845–854.
[52] C. Oostenbrink, A. Villa, A.E. Mark, W.F. Van Gunsteren, A biomolecular force field based on the free enthalpy of hydration and solvation: the GROMOS force-field parameter sets 53A5 and 53A6, J. Comput. Chem. 25 (2004) 1656–1676.